Article

Anti-Perovskite Li-Battery Cathode Materials.

Kwing To Lai, Iryna Antonyshyn, Yurii Prots, and Martin Valldor

J. Am. Chem. Soc., **Just Accepted Manuscript** • Publication Date (Web): 23 Jun 2017

Anti-Perovskite Li-Battery Cathode Materials.

Kwing To Lai,† Iryna Antonyshyn, Yurii Prots, and Martin Valldor*,‡

Max Planck Institute for Chemical Physics of Solids, Nöthnitzer Straße 40, DE-01187 Dresden, Germany

ABSTRACT: Through single-step solid-state reactions, a series of novel bichalcogenides with the general composition $(Li_2Fe)ChO$ (*Ch* = S, Se, Te) are successfully synthesized. $(Li_2Fe)ChO$ (*Ch* = S, Se) possess cubic *anti*-perovskite crystal structures, where Fe and Li are completely disordered on a common crystallographic site (3*c*). According to Goldschmidt calculations, Li^+ and Fe^{2+} are too small for their common atomic position and exhibit large thermal displacements in the crystal structure models, implying high cation mobility. Both compounds $(Li_2Fe)ChO$ (*Ch* = S, Se), were tested as cathode materials against graphite anodes (single cells); They perform outstandingly at very high charge rates (270 mA g^{-1}, 80 cycles) and, at a charge rate of 30 mA g^{-1}, exhibit charge capacities of about 120 mA h g^{-1}. Compared to highly optimized $Li_{1-x}CoO_2$ cathode materials, these novel *anti*-perovskites are easily produced at cost reductions by up to 95 % and, yet, possess a relative specific charge capacity of 75 %. Moreover, these iron-based *anti*-perovskites are comparatively friendly to the environment and $(Li_2Fe)ChO$ (*Ch* = S, Se) melt congruently; the latter is advantageous for manufacturing pure materials in large amounts.

1. Introduction

Energy storage materials represent one of the most important research topics today and the focus is on solid-state rechargeable batteries, as a result of their relative safe use and long-life expectancy. Presently, Li-ion batteries receive most attention because they have high charge density. Although the demand for more efficient batteries in mobile technologies steadily grows, our stand-point is almost 15 years old concerning the battery cathode,[1–2] so the present call in 2017 is the development of new electrode materials.[3–4] At present, advanced Li-battery cathode materials like olivine type $Li_{1-x}FePO_4$,[5] delafossite structured $Li_{1-x}TMO_2$ (*TM* = Co,[6] Mn[7]), and spinel $Li_{1+x}Mn_2O_4$[8] are used. To readily extract and insert Li^+ ions, the host-lattices have to allow for cation migration: $Li_{1-x}FePO_4$ has Li^+-filled 1-D tunnels, $Li_{1-x}CoO_2$ has a 2-D layer-like crystal structure with Li^+ ions between two adjacent CoO_2-layers, and $Li_{1+x}Mn_2O_4$ is a 3-D structure where Li^+ enters interstitial sites. All three have high charge capacity per weight, but they differ in other aspects; $Li_{1-x}FePO_4$ is cheap and non-hazardous but the Li^+ migration is hampered by Li–Fe disorder,[9] which decreases battery life-times and charge/discharge rates. $Li_{1-x}CoO_2$ can be charged/discharged at high rates but is very expensive due to limited resources of environmentally unfriendly cobalt. $Li_{1+x}Mn_2O_4$ is cheap and work at high charging rates but the working voltage causes irreversible deterioration of battery parts.[10] Other oxide candidate materials have significantly less charge density or lower charge rates, making them unsuitable for applications. Non-oxide Li-sulphur battery materials are being developed[11] but they have short battery life-times connected to irreversible, dual migration of sulphur and lithium.[12]

In solid-state *anti*-structures, anions and cations have literally switched places: this way is classic perovskite $SrTiO_3$[13] *inversely* related to *anti*-perovskites, like zero-thermal-expansion material $Mn_3(Ge_{0.5}Cu_{0.5})N$,[14] superconductor Ni_3MgC,[15] and superionic conductors Ag_3SI,[16] Li_3BrO, and Li_3ClO.[17–18] Recently, a new type of cation vacancy ordered *anti*-perovskite, $(Fe_2\square)SeO$ ($\square$ = vacancy) was discovered.[19] Given the fact that Br^-, as in Li_3BrO, has a similar ionic size as Se^{2-},[20] the new battery materials $(Li_2Fe)ChO$ (*Ch* = S, Se, Te) were discovered, and the first investigations thereof will be presented here.

2. Methods

2.1. Materials synthesis. For the solid-state reactions of the Li-containing *anti*-perovskites, x-ray pure Li_2O precursor was obtained by thermal decomposition of LiOH (Alfa Aesar, 98 %) according to Brauer.[21] All quaternaries were synthesized by the same reaction: $Li_2O + Fe + Ch \rightarrow (Li_2Fe)ChO$, with Fe (Alfa Aesar, 3N), S (Alfa Aesar, 99.5 %), Se (Alfa Aesar, 5N), and Te (Alfa Aesar, 4N). The constituents were mixed in an agate mortar and subsequently pressed into pellets. All pellets were placed in corundum crucibles (Aliaxis, Frialit-Degussit, AL23) that were loaded into silica ampoules (QSIL AG Quarzschmelze, Ilmenau) and temporarily shut with a rubber stopper. Outside the glovebox, the ampoules were attached to a turbo-rotary pump station and subsequently sealed when the inner pressure was below 10^{-4} mbar. All samples were heated up to about 750 °C at a rate of 50 °C h^{-1}. This temperature was held for 2–10 hours before quenching in water. The resulting pellets appeared black but turned dark-brown on grinding. All preparations and sample handling were done in an Ar-filled glove box with O_2 and H_2O levels below 1 ppm (MBraun).

2.2. Materials characterization. Powder x-ray diffraction measurements were performed using Guinier cameras

(Huber) equipped with an image-plate detector using a Co$K\alpha_1$ x-ray source. Powdered (Li_2Fe)SO sealed in a silica capillary was investigated at the beamline ID22 at the European Synchrotron Radiation Facility (ESRF) in Grenoble (France). A single crystal of (Li_2Fe)SeO mounted inside an argon filled thin-walled silica capillary was investigated on a Rigaku AFC7 diffractometer with a CCD camera as detector (Saturn 724+) and a Mo$K\alpha$ x-ray source. The software JANA2006[22] was used to compare observed diffraction data with structural model patterns. Thermal analyses were performed with a STA449C (NETZSCH) inside a glove box (MBraun). For elemental analyses by inductively coupled plasma-optical emission spectroscopy (ICP-OES) on a matrix matched calibrated Vista RL (Varian), the samples were digested with a solution of ethylene-diaminetetraacetic acid (EDTA, 3.5 mL 0.02 M) and acid mixture (2.5 mL HCl:HNO_3, 1:1) in a turboWAVE (MLS-GmbH) at 120 °C for 15 minutes. The solutions were then transferred to 50 mL volumetric flasks and filled with ultrapure water.

2.3. Electrochemical measurements. Aluminium and copper plates were used as current collectors for cathode and anode, respectively. For preparation of slurries, the battery cathode material (Li_2Fe)*Ch*O (*Ch* = S, Se) or anode graphite (Alfa Aesar, 99.8 %, ~325 mesh) was mixed with carbon black (Alfa Aesar, acetylene compressed, 99.9+ %, S>A, 75 $m^2\ g^{-1}$, bulk density 80–120 g L^{-1}), and polyvinylidene fluoride (PVdF, Sigma Aldrich) in mass ratio 85:5:10 inside the organic solvent N-methylpyrrolidone (NMP, Sigma Aldrich, anhydrous, 99.5 %). All slurries were manually distributed on respective metallic plate (~25 cm^2) with subsequent heating at 100 °C during 1–2 hours for organic solvent (NMP) removal. About 0.3 grams of active material was used for each trial battery. A separator of non-woven material (Freudenberg, FS2226) was wetted with commercially available 1.0 M $LiPF_6$ in ethylene carbonate (EC) and ethyl methyl carbonate (EMC) mixture (50:50 by volume, Sigma Aldrich). The battery set-up was placed in plastic bag with additional amounts of electrolyte. All preparations and electrochemical measurements were performed in an Ar-filled glove box (MBraun) using a BioLogic SP300 potentiostat.

3. Results

3.1. Reaction products. For polycrystalline samples, a thermal quenching after the main reaction proved necessary to prevent partial decomposition of each *anti*-perovskite into binaries, like Li_2Ch and iron oxides. All obtained powders appeared dark red-brown while small crystals were black. In all syntheses, there were no obvious reactions between sample and crucible or silica tube. The decomposition into binaries was much less obvious for single crystals, as obtained by melting, although cooled at much lower rates. A tentative explanation would be that the decomposition into binaries initiates at crystallite surfaces and its rate is proportional to the sample surface area. X-ray diffraction data from single crystalline (Li_2Fe)SeO (Table S1, Supporting Information) and powder data of (Li_2Fe)*Ch*O (*Ch* = S, Se, Figure 1a,b) indicate that both are cubic anti-perovskites (Figure 2a) described by the space group $Pm\bar{3}m$. (Table S2, Supporting Information). Accordingly, Li and Fe are randomly distributed while sharing the same positions on the atomic lattice. (Li,Fe) and *Ch* together form a cubic close-packing where O^{2-} ions occupy octahedral voids.

Powder x-ray diffraction data of (Li_2Fe)TeO (Figure 1c) are well described with an 4H-hexagonal *anti*-perovskite structure model (Figure 2b), inversely related to that of $BaCrO_3$.[23] Going from cubic (*Ch* = S, Se) to hexagonal (*Ch* = Te) perovskites, the condensation of octahedra increases, going from purely vertex-sharing to partly face-sharing. Consequently, the lattice dimensionality changes drastically (Figure 2). There are two different cation sites in Li_2FeTeO: one site is fully occupied by Li and the other site contains a Li/Fe mixture (Figure 2b). O^{2-} occupies two neighbouring octahedral voids in a hexagonal close-packing of Li–Fe–Te.

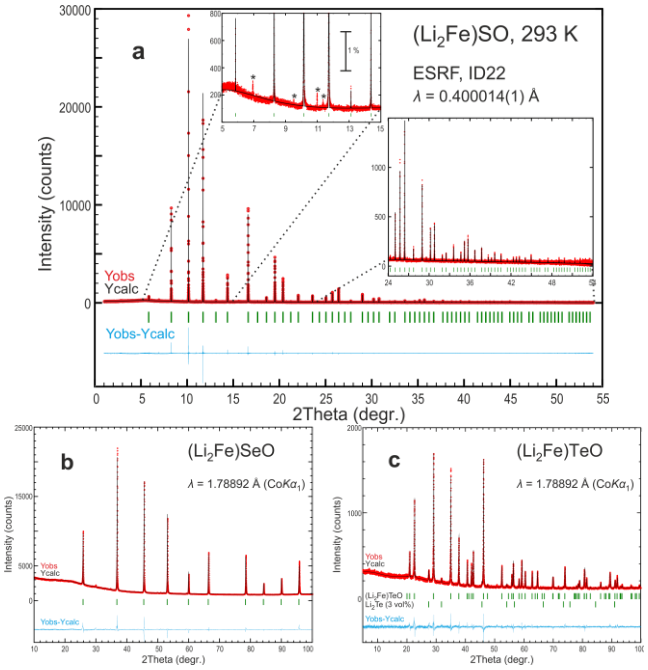

Figure 1. (a) Synchrotron x-ray diffraction powder pattern of (Li_2Fe)SO and laboratory camera powder x-ray diffraction data of (b) (Li_2Fe)SeO and (c) (Li_2Fe)TeO. In (a), insets show the high angle range (down) and intensities from secondary phases (up), marked with asterisks, with a bar corresponding to 1 % of the maximum diffraction intensity.

Single-step syntheses result in highly crystalline materials of at least 95% purity as estimated from x-ray powder diffraction data (Figure 1). Unit cell volumes, as normalised per formula unit (f.u.), increase expectedly through S–Se–Te (59.871(2), 63.977(2), 75.068(3) $Å^3$ $f.u.^{-1}$). To analyse relative atomic compositions, also with respect to electron poor lithium, complementary inductively coupled plasma-optical emission spectroscopic (ICP-OES) analyses were performed; All results strongly support the proposed compositions (S4, Supporting Information).

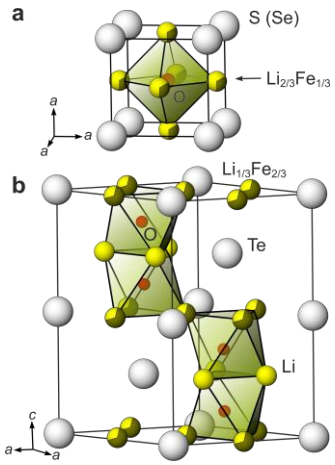

Figure 2. (a) Cubic *anti*-perovskites $(Li_2Fe)ChO$ (*Ch* = S, Se) and (b) 4H-hexagonal *anti*-perovskite $(Li_2Fe)TeO$ with emphasized octahedra around oxygen.

3.2. Thermodynamic investigations. Under inert conditions, an as-prepared powder of $(Li_2Fe)SeO$ melts congruently at 1020 °C and re-solidifies at 1000 °C (Figure 3). X-ray powder diffraction data confirm that there is no phase deterioration at 1000 °C and those of a melted and re-crystallised sample (heated to 1250 °C) indicate only tiny amounts of secondary phases (Figure S5, Supporting Information). The identical unit cell size of pristine and melted samples also supports the congruent-melt scenario. A similar behaviour is observed for $(Li_2Fe)SO$ (Figures S5–S6, Supporting Information) but its melting temperature is 980 °C. The first order transition with only minor weight change for $(Li_2Fe)ChO$ (*Ch* = S, Se) is a great advantage for preparative works.

A slow deterioration of $(Li_2Fe)ChO$ (*Ch* = S, Se) in air is clearly visible by eye, e.g. polycrystalline pieces crumble, and this behavior was investigated: $(Li_2Fe)ChO$ (*Ch* = S, Se) were left at room temperature in controlled, dry air during 5 hours and in normal air with 30 % moisture during 1.5 hours. From subsequent x-ray diffraction investigations (Figures S7–S8, Supporting Information) the reason is clear: $(Li_2Fe)SeO$ endures dry air although oxygen is present, but moist air leaches Li from the investigated phase according to: $(Li_2Fe)SeO + 3x/2\ H_2O + x/4\ O_2 \rightarrow (Li_{2-x}Fe)SeO + x\ Li(OH)(H_2O)$. $(Li_2Fe)SO$ reacts even more pronounced with moist air (Figures S7–S8, Supporting Information). This means that water moisture in combination with oxygen is the true reason for deterioration of our novel Li-based *anti*-perovskites at room temperature.

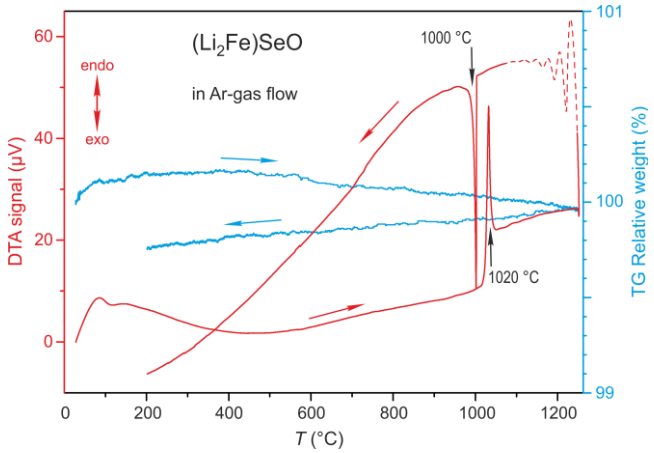

Figure 3. Differential thermal analysis (DTA) and thermogravimetric (TG) data of $(Li_2Fe)SeO$ in flowing argon gas, where arrows mark curve anomalies and measuring directions. An instrumental DTA curve feature is dashed.

3.3. Electrochemical Li-charge/discharge. In a battery set up with *anti*-perovskite $(Li_2Fe)SeO$ as cathode and graphite as anode, the charging can be described with the general reaction: $(Li_2Fe)SeO + nC(graphite) \dashrightarrow (Li_{2-x}Fe)SeO + Li_xC_n$. Thereby changes the average oxidation state of Fe from +2 to +(2+*x*). During battery discharge, this reaction is reversed. The Li extraction from the cathode is often assumed to be rate limiting for charge/discharge processes. Crystal structure investigations, presented above, cannot distinguish between dynamic or static Li–Fe disorder. However, the structurally related *anti*-perovskites Li_3BrO and Li_3ClO are reported to have dynamic Li disorder and remarkable Li^+-ionic conducting properties.[17–18] A $(Li_2Fe)SeO$ – graphite battery (Figure S9, Supporting Information) was extensively tested and the highest specific charge current was 270 mA g^{-1} (Figure 4); During 10 charge/discharge cycles, there is no deterioration of the battery (Figure 4) and the specific charge capacity (about 60 mAh g^{-1}) remains almost constant during 80 cycles (Figure S9, Supporting Information).

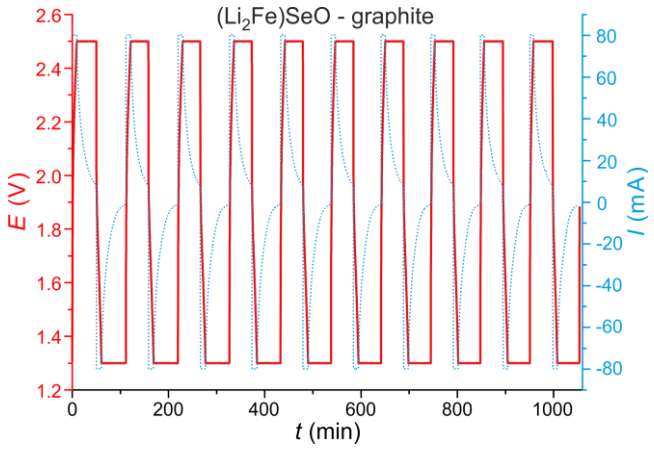

Figure 4. Ten charge/discharge curves of a $(Li_2Fe)SeO$ – graphite battery.

For an electrochemical extraction up to $x = 1$, which would result in (LiFe)SeO, the theoretical charge density

would be $Q_{max} = nF(3600M)^{-1} = 162.8$ mA h g^{-1}, where n is the number of Li^+ ions in moles, F is the Faraday constant = 96485 s A mol^{-1}, and M is the molar mass of $(Li_2Fe)SeO$ = 164.69 g mol^{-1}. By the same calculation, $(Li_2Fe)SO$ theoretically reaches even higher values of 227 mA h g^{-1} (Figure S10, Supporting Information). This can be compared with experimental (theoretical) values of 160 (274) mA h g^{-1} for $Li_{1-x}CoO_2$.[24] The reason for presuming the stability of 50 % delithiated (Li□Fe)*Ch*O (□ = vacancy, *Ch* = S, Se) is the existence of cation vacant $(Fe_2□)SeO$,[19] where one third of the cations are missing without crystal structure break-down. Performed charges/discharges indicate that about 3/4 of the theoretical charge was already obtained for $(Li_2Fe)SeO$: 120 mA h g^{-1} at a rate of about 30 mA g^{-1} = 0.25C (Figure S9, Supporting Information). The size of the atomic lattice (unit cell parameter *a*) does not change significantly for a charged (delithiated) material (Figure S11, Supporting Information), which is a good indication of advantageous, negligible lattice strain (volume change) for charge/discharge processes.

4. Discussions

To estimate the Goldschmidt tolerance factor[13] for the two cubic title compounds, an average ionic radius was assumed for the (Li_2Fe)-site. The calculated tolerance factors and the ideal cubic cell parameters are smaller than observations (Figure S12, Supporting Information). This suggests relatively large voids for the cations to occupy and agrees with the extraordinary Li migration rate and thermal atomic displacements in crystal structure descriptions.

As compared to delafossites Li*TM*O_2 (*TM* = Co,[6] Mn,[7] Ni), the cubic *anti*-perovskite title compounds have +2 pristine oxidation states of Fe while *TM* is +3 in delafossites. This lowers the work potential window for *anti*-perovskite cathodes, and standard battery constituents remain stable: the *anti*-perovskites can be charged/discharged without destroying anodes or electrolytes. This is advantageous in comparison with high-voltage cathodes, like $Li_{1+x}Mn_2O_4$,[8] where a thermal run-away, due to over voltage, decomposes the fluorine based electrolytes, which are discussed as potential hazards for users and environment.[25] Nevertheless, the working voltage of *anti*-perovskite batteries can be designed by selecting another anode materials instead of graphite; this might increase the battery voltage and, thus, offer even higher energy densities.

The cubic title compounds allow for isotropic 3D Li^+ migration, which is similar to the situation in $Li_{1+x}Mn_2O_4$,[8] but more advantageous than Li^+ migrations in layers of $Li_{1-x}(Co,Mn)O_2$[6-7] and in columns of $Li_{1-x}FePO_4$[5] (Figure 5). The isotropic Li migration in investigated *anti*-perovskites is stable against minor crystallographic faults, in contrast to the high fault-sensitivity in $Li_{1-x}FePO_4$.[9] Moreover, due to the structural similarities, an all-solid battery is possible with any of the cubic title compounds as cathode, Li_3XO (*X* = Cl, Br)[17-18] as electrolyte, and an anode of perhaps Fe_2SeO.[19] Lattice mismatches would be small and techniques such as molecular beam epitaxy or laser ablation might be applied for making ultra-thin batteries with neither polymer matrices nor liquid electrolytes. Alternatively, the recently reported solid-state electrolyte, involving Li-glass,[26] can be used between the anode and the cathode.

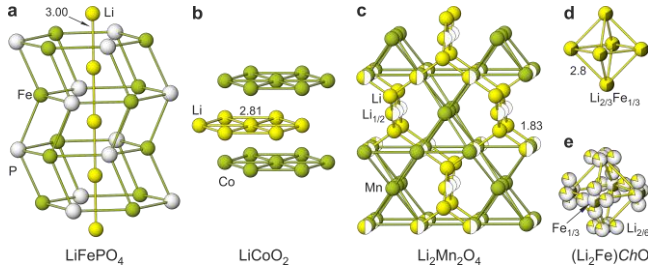

Figure 5. Li^+ migration paths in (a) olivine $LiFePO_4$, (b) delafossite $LiCoO_2$, (c) spinel $Li_2Mn_2O_4$, (d) *anti*-perovskite $(Li_2Fe)ChO$ (*Ch* = S, Se), and (e) *anti*-perovskite $(Li_2Fe)SeO$ with refined Li split-positions. All anions have been omitted for clarity and the shortest distances (in Å) between two adjacent Li-sites are marked. Partial occupied sites are indicated with corresponding filling of atom spheres.

There are further promising Li-battery cathode materials that are still being optimized. For example, $Li_xV_2O_5$, where *x* can be even up to 3,[27] has a very high charge density but low charge rates, which were improved by increasing the active surface[28] or implementing it in a glassy composite.[29] Unfortunately, the high charge capacity can only be retained over few charge/discharge cycles. Moreover, vanadium is relatively expensive and its oxides are harmful to the environment. In contrast, both Li_2MnO_3[30] and FeF_3[31] are environmentally viable and are also candidates for the use as battery cathodes due to low costs and high energy densities. However, both compounds suffer from strongly fading charge capacities during charge/discharge cycling, despite the extensive topology optimizations, e.g. nano-wires of FeF_3[32] and nano-structured Li_2MnO_3.[33] In contrast, the cubic title compounds exhibit only faint capacity loss during 80 charge/discharge cycles at high rates. However, even longer experiments have to be performed to establish the long-term stability of *anti*-perovskite cathodes.

In conclusion, our novel *anti*-perovskites can be readily produced, are environmentally friendly, and perform well enough as Li-battery cathodes to compete with $Li_{1-x}CoO_2$. $(Li_2Fe)ChO$ (*Ch* = S, Se) can be charged at high rates and the material cost for $(Li_2Fe)SO$ is reduced by about 95 % in comparison to $Li_{1-x}CoO_2$. Hence, at viable costs and with less environmental issues, the cubic *anti*-perovskite title compounds can be used in larger energy storage stations or power vehicles safely.

ASSOCIATED CONTENT

Supporting Information. Crystal structure models based on single crystal and powder x-ray data, CIF-file of $(Li_2Fe)SO$, CIF-file of $(Li_2Fe)SeO$, ICP-OES data, $(Li_2Fe)SO$ DTA/TG data, x-ray data on melted samples, x-ray data on samples that were left in dry air or in moist air, x-ray data on partly and highly charges states of cathode material, charge/discharge curves,

battery specific capacities. This material is available free of charge via the Internet at http://pubs.acs.org.

AUTHOR INFORMATION

Corresponding Author

*E-mail: martin.valldor@cpfs.mpd.de or m.valldor@ifw-dresden.de.
ORCID: 0000-0001-7061-3492

Present Addresses

† Department of Physics, The Chinese University of Hong Kong, Shatin, Hong Kong
‡ Leibniz Institute for Solid State and Materials Research, Helmholtzstraße 20, DE-01069 Dresden, Germany

Author Contributions

All authors have given approval to the final version of the manuscript.

ACKNOWLEDGMENT

We thank Marcus Schmidt and Susann Scharsach for thermal analyses, Gudrun Auffermann for elemental analyses, and Mauro Coduri for assistance at ESRF. Liu Hao Tjeng and Juri Grin are acknowledged for their invaluable support and help.

REFERENCES

(1) Tarascon, J. -M.; Armand, M. *Nature* **2001**, *414*, 359–367.
(2) Evarts, E. C. *Nature* **2015**, *526*, S93–S95.
(3) Grey, C. P.; Tarascon, J. -M. *Nat. Mater.* **2017**, *16*, 45–56.
(4) Chu, S.; Cui, Y.; Liu, N. *Nat. Mater.* **2017**, *16*, 16–22.
(5) Pahdi, A. K.; Najundaswamy, K. S.; Goodenough, J. B. *J. Electrochem. Soc.* **1997**, *144*, 1188–1194.
(6) Mizushima, K.; Jones, P. C.; Wiseman, P. J.; Goodenough, J. B. *Mater. Res. Bull.* **1980**, *15*, 783–789.
(7) Armstrong, A. R.; Bruce, P. G. *Nature* **1996**, *381*, 499–500.
(8) Thackeray, M. M.; David, W. I. F.; Bruce, P. G.; Goodenough, J. B. *Mater. Res. Bull.* **1983**, *18*, 461–472.
(9) Wang, J.; Chen-Wiegart, Y. K.; Wang, J. *Nat. Commun.* **2014**, *5*, 4570.
(10) Tarascon, J. M.; Guyomard, D. *Electrochim. Acta* **1993**, *38*, 1221–1231.
(11) Rauh, R. D.; Abraham, K. M.; Pearson, G. F.; Surprenant, J. K.; Brummer, S. B. *J. Electrochem. Soc.* **1979**, *126*, 523–527.
(12) Manthiram, A.; Fu, Y.; Su, Y. –S. *Acc. Chem. Res.* **2013**, *46*, 1125–1134.
(13) Goldschmidt, V. M. *Sci. Nat.* **1926**, *14*, 477–485.
(14) Song, X.; Sun, Z.; Huang, Q.; Rettenmayr, M.; Liu, X.; Seyring, M.; Li, G.; Rao, G.; Yin, F. *Adv. Mater.* **2011**, *23*, 4690–4694.
(15) He, T.; Huang, Q.; Ramirez, A. P.; Wang, Y.; Regan, K. A.; Rogado, N.; Hayward, M. A.; Haas, M. K.; Slusky, J. S.; Inumara, K.; Zandbergen, H. W.; Ong, N. P.; Cava, R. J. *Nature* **2001**, *411*, 54–56.
(16) Reuter, B.; Hardel, K. *Sci. Nat.* **1961**, *48*, 161–161.
(17) Zhao, Y.; Daemen, L. L. *J. Am. Chem. Soc.* **2012**, *134*, 15042–15047.
(18) Emly, A.; Kioupakis, E.; van der Ven, A. *Chem. Mater.* **2013**, *25*, 4663–4670.
(19) Valldor, M.; Wright, T.; Fitch, A.; Prots, Yu. *Angew. Chem., Int. Ed.* **2016**, 55, 9380–9383.
(20) Shannon, R. D. *Acta Crystallogr.* **1976**, *A32*, 751–767.
(21) Brauer, G. *Handbuch der Präparativen Anorganischen Chemie*, Ferdinand Elke Verlag, Stuttgart, Germany **1978**, 950–951.
(22) Petříček, V.; Dušek, M.; Palatinus, L. *Z. Kristallogr.* **2014**, *229*, 345–352.
(23) Chamberland, B. L. *J. Solid State Chem.* **1982**, *43*, 309–313.
(24) Cho, W.; Myeong, S.; Kim, N.; Lee, S.; Kim, Y.; Kim, M.; Kang, S. J.; Park, N.; Oh, P.; Cho, J. *Adv. Mater.* **2017**, 1605578.
(25) Hammami, A.; Raymond, N.; Armand, M. *Nature* **2003**, *424*, 635–636.
(26) Braga, M. H.; Grundish, N. S.; Murchinson, A. J.; Goodenough, J. B. *Energy Environ. Sci.* **2017**, *10*, 331–336.
(27) Delmas, C.; Cognac-Auradou, H.; Cocciantelli, J. M.; Ménétrier, M.; Doumerc, J. P. *Solid State Ionics* **1994**, *69*, 257–264.
(28) Passerini, D. B. Le; Guo, J.; Ressler, J.; Owens, B. B.; Smyrl, W. H. *J. Electrochem. Soc.* **1996**, *143*, 2099–2104.
(29) Afyon, S.; Krumeich, F.; Mensing, Ch.; Borgschulte, A.; Nesper, R. *Sci. Rep.* **2014**, *4*, 7113.
(30) Boulineau, A.; Croguennec, L.; Delmas, C.; Weill, F. *Chem. Mater.* **2009**, *21*, 4216–4222.
(31) Li, H.; Balaya, P.; Maier, J. *J. Electrochem. Soc.* **2004**, *151*, A1878–A1885.
(32) Li, L.; Meng, F.; Jin, S. *Nano Lett.* **2012**, *12*, 6030–6037.
(33) Liu, G.; Zhang, S. *Int. J. Electrochem. Sci.* **2016**, *11*, 5545–5551.

SYNOPSIS TOC

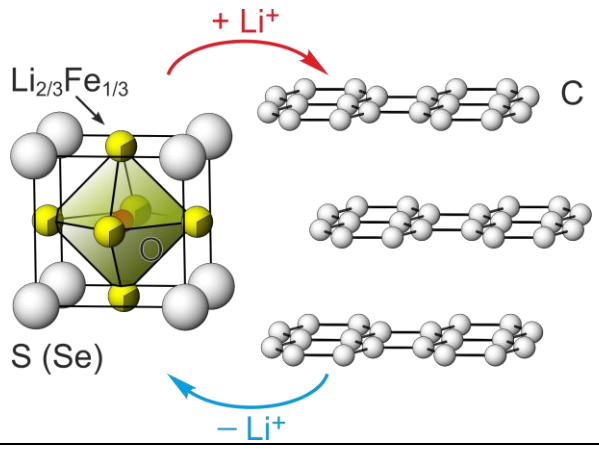

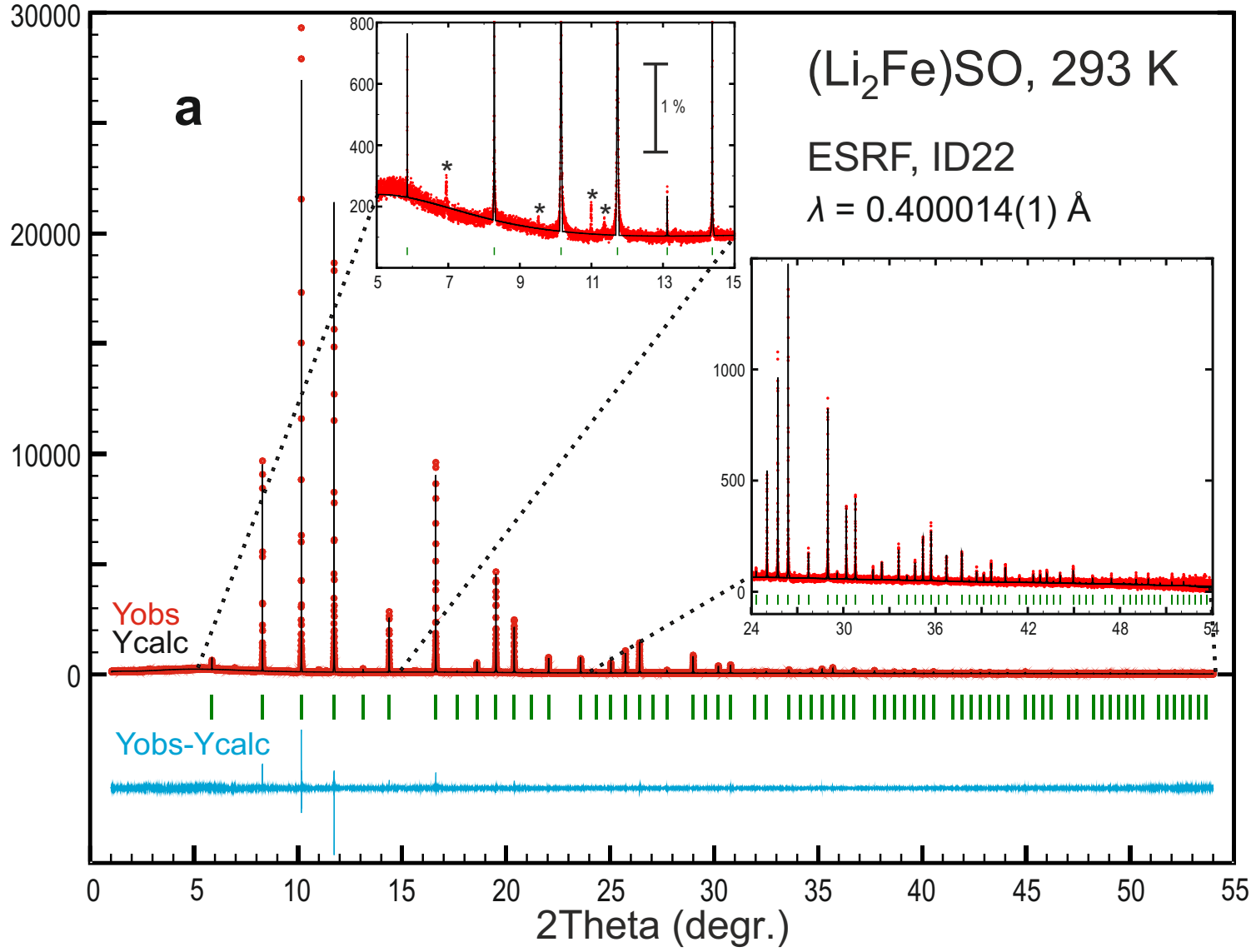
a
(Li2Fe)SO, 293 K
ESRF, ID22
λ = 0.400014(1) Å
Yobs
Ycalc
Yobs-Ycalc
1 %
Intensity (counts)
2Theta (degr.)

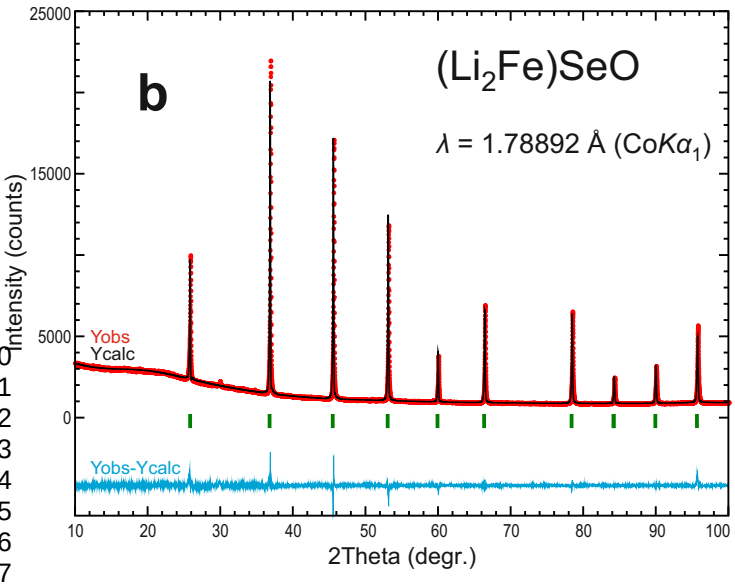
b
(Li2Fe)SeO
λ = 1.78892 Å (CoKα1)
Intensity (counts)
Yobs
Ycalc
Yobs-Ycalc
2Theta (degr.)

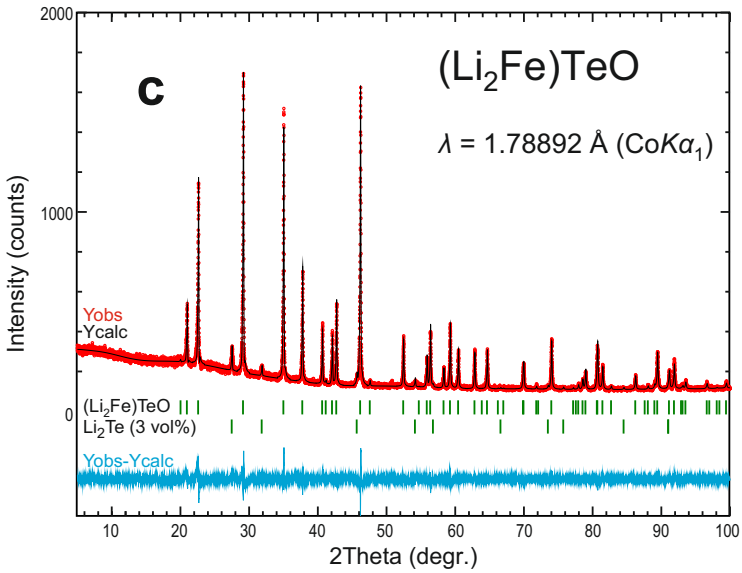
c
(Li2Fe)TeO
λ = 1.78892 Å (CoKα1)
Intensity (counts)
Yobs
Ycalc
(Li2Fe)TeO
Li2Te (3 vol%)
Yobs-Ycalc
2Theta (degr.)

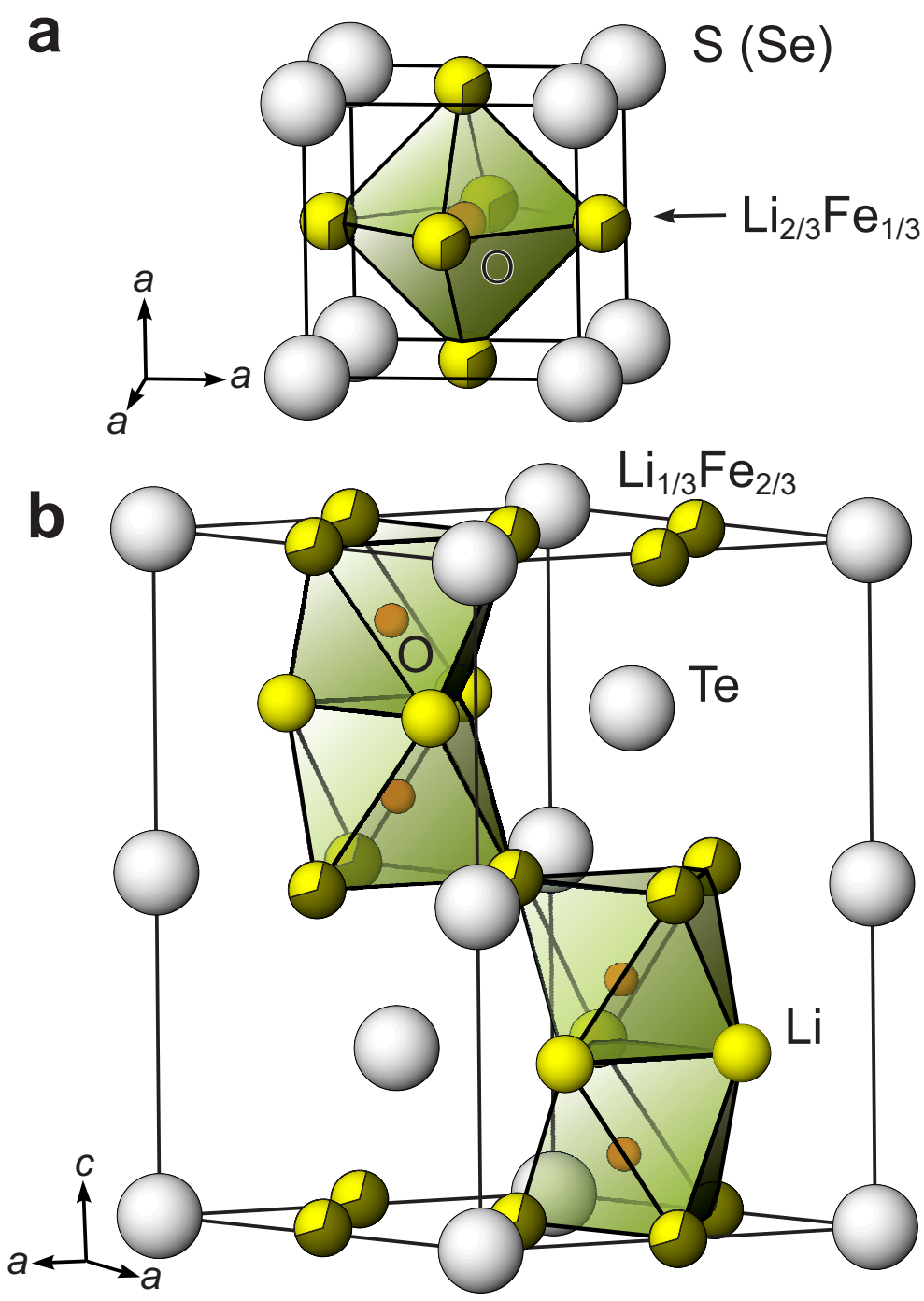
a
S (Se)
$Li_{2/3}Fe_{1/3}$
O
a
a
a
b
$Li_{1/3}Fe_{2/3}$
O
Te
Li
c
a
a

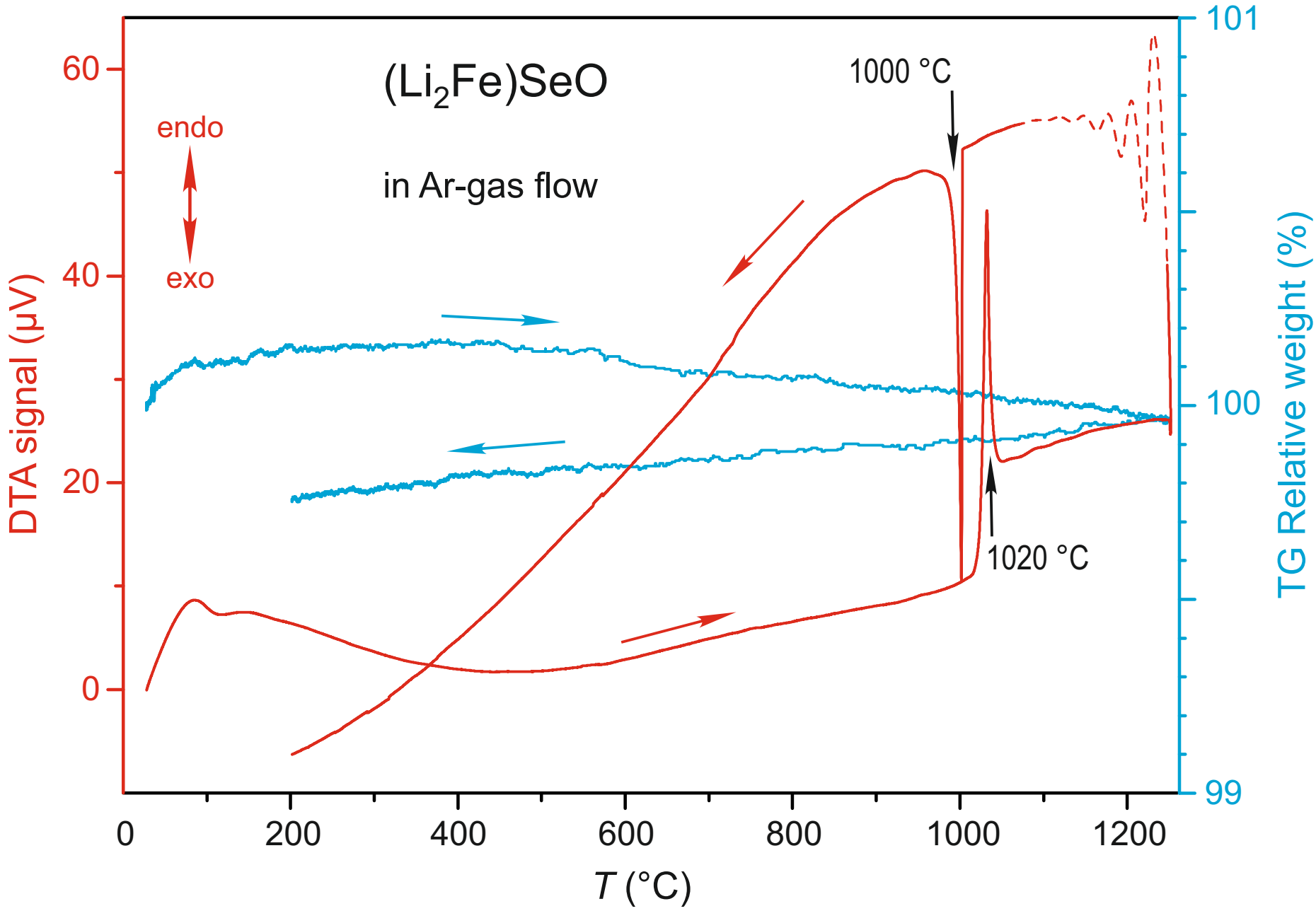
(Li2Fe)SeO
in Ar-gas flow
endo
exo
1000 °C
1020 °C
DTA signal (µV)
TG Relative weight (%)
T (°C)
60
40
20
0
101
100
99
0
200
400
600
800
1000
1200

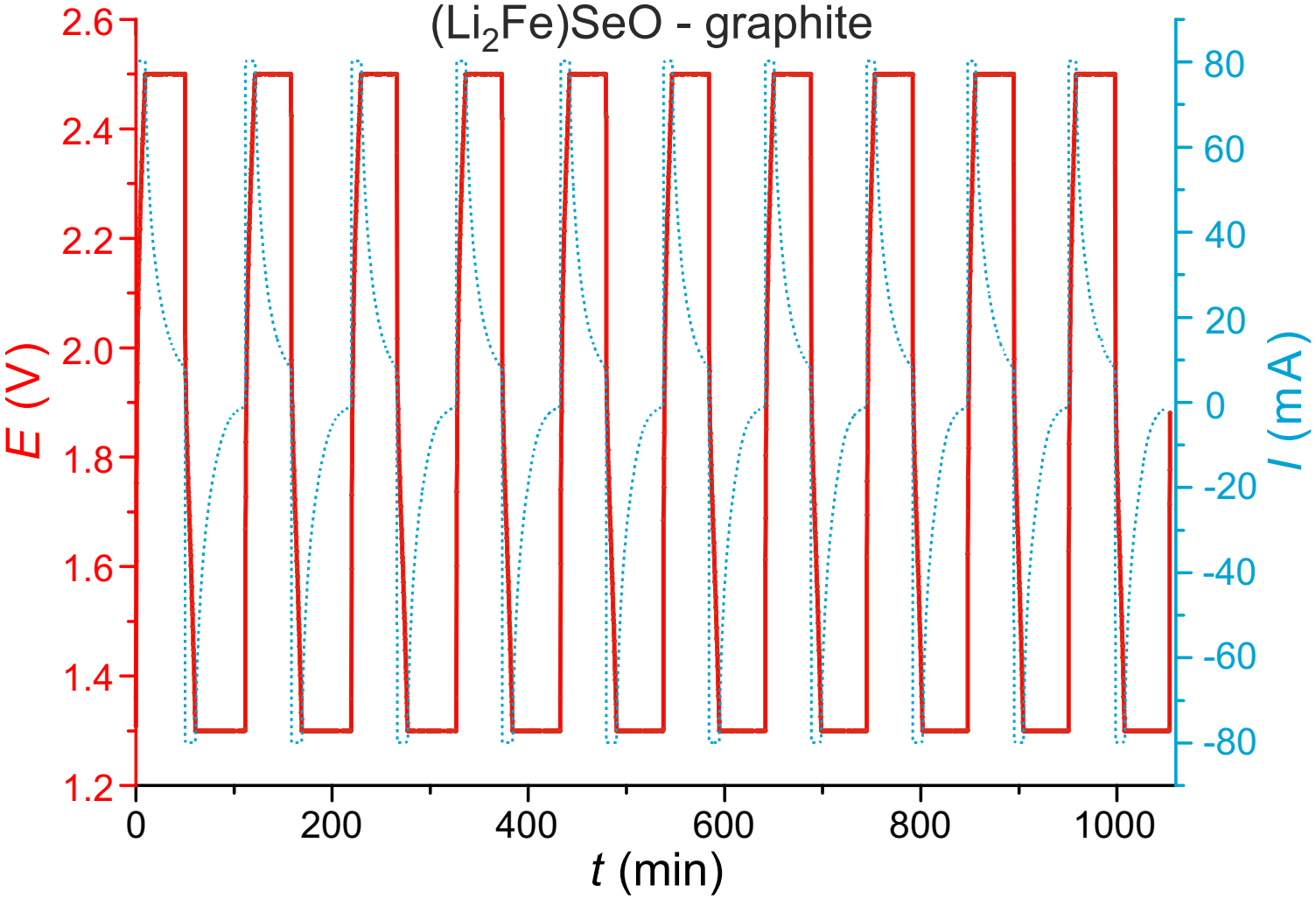
(Li2Fe)SeO - graphite
E (V)
I (mA)
t (min)
2.6
2.4
2.2
2.0
1.8
1.6
1.4
1.2
80
60
40
20
0
-20
-40
-60
-80
0
200
400
600
800
1000

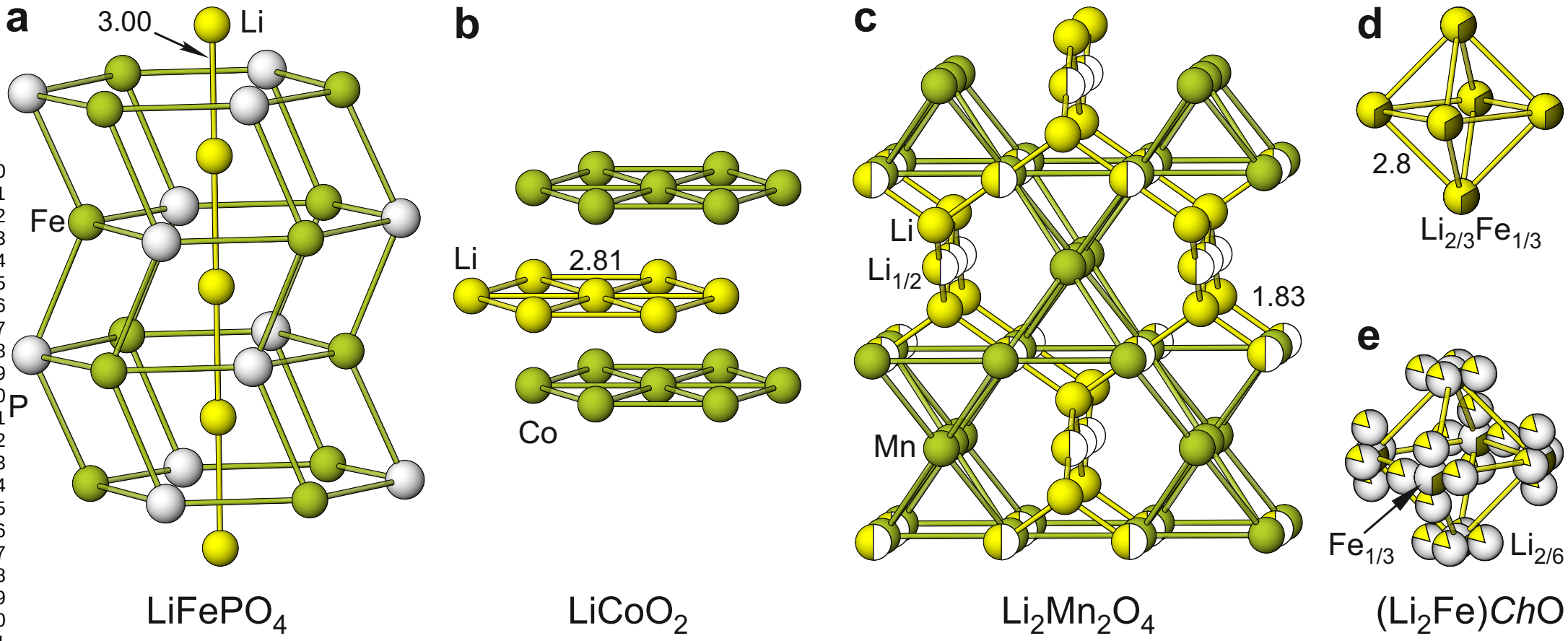
a
3.00
Li
Fe
P
b
Li
2.81
Co
c
Li
Li1/2
1.83
Mn
d
2.8
Li2/3Fe1/3
e
Fe1/3
Li2/6
LiFePO4
LiCoO2
Li2Mn2O4
(Li2Fe)ChO

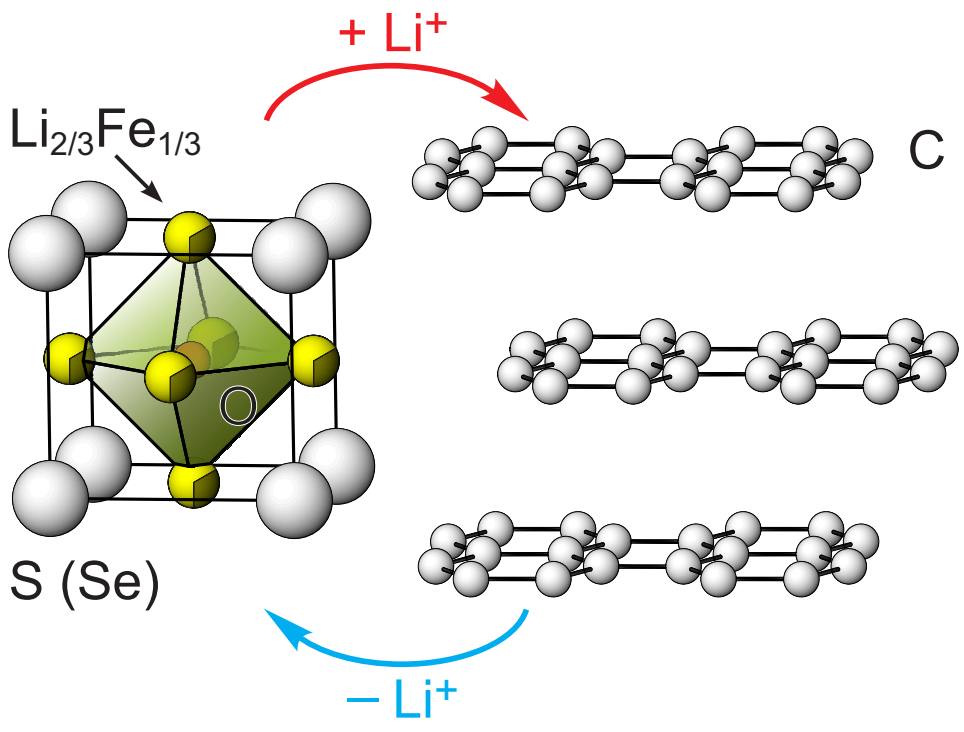
+ Li+
Li2/3Fe1/3
C
S (Se)
– Li+